CHEMISTRY OF MATERIALS

ARTICLE

pubs.acs.org/cm

Mesoporous Aluminosilicates from a Zeolite BEA Recipe

Eric Masika and Robert Mokaya*

School of Chemistry, University of Nottingham, University Park, Nottingham NG7 2RD, United Kingdom

Supporting Information

ABSTRACT: We report the unusual formation of mesoporous aluminosilicates with enhanced properties from a zeolite recipe. The mesoporous aluminosilicates were prepared from a recipe typically used for the synthesis of microporous zeolite BEA. The key to the formation of a mesostructured material is use of a relatively low crystallization temperature and in particular a high Si/TEAOH ratio in the synthesis gel. The porosity of the aluminosilicates may be further modified by simple washing/refluxing (in water) steps performed on either the as-synthesized mesophase or the calcined material. This allows preparation of aluminosilicate materials that possess tunable mesoporosity with surface areas of 500−850 m^2/g, pore volumes in the range of 0.35−1.5 cm^3/g, and pore sizes between 25 and 140 Å. Depending on their synthesis temperature, the mesoporous aluminosilicates contain some zeolite building units within their framework and possess strong acid sites and high hydrothermal stability.

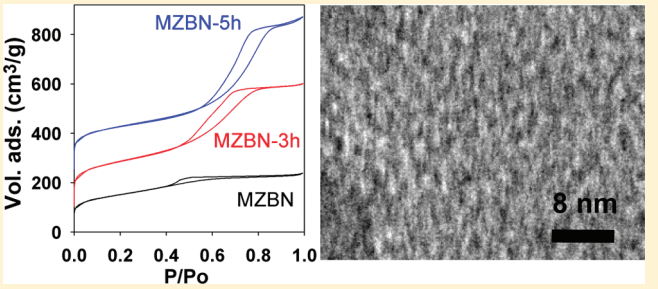

KEYWORDS: mesoporous, aluminosilicate, zeolite β, zeolite building units, hydrothermal stability

INTRODUCTION

Crystalline microporous zeolites are very effective molecular sieves, ion exchangers, and solid acid catalysts. Microporous zeolites are prepared via so-called molecular templating wherein a single organic or ionic species act as a template for the formation of ordered pore channels. The molecular templating generates highly ordered (both structural and local) porous materials whose pore size is however limited to some extent by the size of the molecular templates. The pore size of zeolites is therefore limited to below 12 Å and is typically 4−10 Å, which restricts their use as molecular sieves or catalysts in processes that involve large molecules.[1] Larger pore mesoporous materials may be prepared via a variety of supramolecular templating methods whereby arrays of surfactant molecules are used as structure directors.[2] Aluminosilicate zeolites are excellent solid acid materials due to their crystalline pore walls (frameworks) that are ordered at the atomic level, which contrasts with most mesoporous aluminosilicas that have amorphous pore walls.[3,4] Amorphous mesoporous aluminosilicas therefore have several limitations, including poor hydrothermal stability, low and weak acidity, and low ion exchange capacity,[5,6] which limit their use as solid acid catalysts or cation exchangers.

The preparation of crystalline mesoporous aluminosilicas via supramolecular templating is difficult because the preparation conditions required to generate mesoporosity do not generally favor the formation of crystalline aluminosilicate frameworks. Although the formation of supramolecular-templated crystalline silica−surfactant mesophases has been demonstrated in a number of studies,[7−9] their transformation to template-free crystalline materials often fails. Recently, however, mesoporous aluminosilicas with crystallinity were prepared with amphiphilic organosilanes as templates.[10] The formation of mesoporous silicate materials is however not limited to supramolecular templating. Mesoporous silicate composites may be prepared using small organic molecules as "structure-directing agents", wherein the mesoporous structure formation mechanism is different from that which applies for supramolecular templates.[11,12] However, in most cases the resulting materials are composites made up of zeolite crystallites embedded in a disordered mesoporous matrix.[12] It has been suggested that the disordered mesopores in such composites are generated via a nontemplating structure-directing mechanism.[12c]

The work presented here explores the preparation of mesoporous aluminosilicates using template molecules and synthesis conditions that are normally used for the preparation of crystalline zeolites. The aim is to achieve the formation of mesostructured aluminosilicates that exhibit properties associated with zeolites, such as strong acidity and thermal/hydrothermal stability. The composition of the synthesis gel and the preparation conditions (i.e., recipe) used are similar to those which are known to generate zeolite BEA.[13] We show that by using such a zeolite recipe it is possible to prepare strongly acidic and hydrothermally stable mesoporous aluminosilicates (designated as MZBN-*X*, where *X* is the crystallization temperature (°C)) that have potential for use as solid acid catalysts or catalyst supports.

EXPERIMENTAL SECTION

Materials Synthesis. In a typical synthesis,[13a] 0.3 g of NaOH and 2.7 g of aluminum isopropoxide were dissolved in 33 mL of water by

Received: March 9, 2011
Revised: March 22, 2011
Published: April 08, 2011

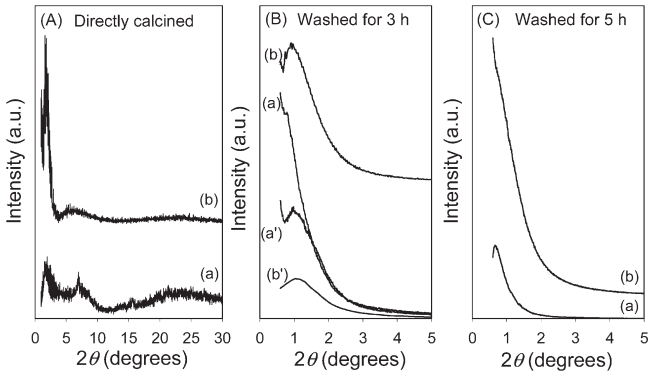

Figure 1. Powder XRD patterns of (a) as-synthesized and (b) calcined MZBN-100 aluminosilicate materials prepared from a zeolite BEA recipe at 100 °C (A) directly calcined (sample MZBN-100), (B) washed for 3 h before calcination (MZBN-100w3h), and (C) washed for 5 h before calcination (MZBN-100w5h). (a′) and (b′) in (B) are for sample MZBN-100w3hd, which was washed in 100 mL of water.

stirring at room temperature, followed by addition of 71 g of tetraethyl orthosilicate and 84 g of tetraethylammonium hydroxide (20 wt % in water) to give a gel of molar composition 0.57NaOH:9TEAOH:Al:25Si:420H_2O, which was placed in a Teflon-lined autoclave and heated at 100 °C for 8 days. The solid product was obtained, without washing, by drying in a fume hood and then either directly calcined in static air at 550 °C for 4 h or washed (stirred) in boiling water for 3 or 5 h and dried before calcination. The sample prepared at 100 °C and calcined directly without washing was designated as MZBN-100. Three samples were washed (stirred) in boiling water before calcination and are designated as follows: MZBN-100w3h (washed in 200 mL of water for 3 h), MZBN-100w3hd (washed in 100 mL of water for 3 h), and MZBN-100w5h (washed in 200 mL of water for 5 h). We also prepared five more sets of samples as described above but at crystallization temperature of 25, 50, 80, 135, and 150 °C. The direct calcination and washing/calcination regime was as described above.

The hydrothermal stability of calcined MZBN-100 materials was tested by refluxing the samples in boiling water for 6 or 120 h at a water-to-sample ratio of 1 L/g. The designation of the refluxed samples is prefixed with R; for example, refluxed MZBN-100 is designated as RMZBN-100.

Characterization. Powder X-ray diffraction (XRD) analysis was performed using a Bruker AXS D8 Advance powder diffractometer with Cu Kα radiation (40 kV, 40 mA), a 0.020° step size, and a 1 s step. The elemental composition (Si/Al ratio) was determined by a Philips MiniPal PW4025 X-ray fluorescence (XRF) instrument. Textural properties were determined via nitrogen sorption analysis at −196 °C using a conventional volumetric technique by a Micromeritics ASAP 2020 sorptometer. Before analysis the samples were oven-dried at 150 °C and evacuated overnight at 150 °C under vacuum. The Brunauer−Emmett−Teller (BET) specific surface area was calculated using the standard BET method for adsorption data in the relative adsorption range from 0.05 to 0.2. The total pore volume was estimated on the basis of the amount of nitrogen adsorbed at a relative pressure (P/P_o) of ca. 0.99. The pore size distribution (PSD) was determined using the Barrett−Joyner−Halenda (BJH) method applied to the adsorption branch of the isotherm. The PSD was also assessed via a nonlocal density functional theory (NLDFT) method using nitrogen adsorption data and assuming a slit pore model. The microporosity was determined by performing *t*-plot analysis of the sorption data. Thermogravimetric analysis was performed using a TA Instruments SDT Q600 analyzer in static air conditions. A Bruker Optics TENSOR 27 series Fourier transform infrared (FT-IR) spectrometer was use to obtain IR spectra. ^{29}Si magic-angle spinning (MAS) nuclear magnetic resonance (NMR) spectra were acquired with a silicon-29 frequency of 59.56 MHz, an acquisition time of 30−50 ms, a total spectral width of 30 kHz, a recyle delay of 30 s, and an MAS rate of 5.1 kHz. ^{27}Al MAS NMR spectra were acquired at a frequency of 104 MHz, an acquisition time of 10 ms, a recycle delay of 0.1 s, a spectral width of 416 kHz, and an MAS rate of 14.0 kHz.

The acid content was determined using established procedures that employ thermal desorption of cyclohexylamine (CHA).[14,15] Samples were exposed to liquid CHA at room temperature, after which they were kept overnight (at room temperature) and then in an oven at 80 °C for 2 h to allow the base to permeate the samples. Thermogravimetric analysis (TGA) curves were then obtained for the CHA-containing samples. The mass loss associated with desorption of the base from acid sites was used to calculate the total the acid content (mmol of CHA/g of sample) assuming that each acid site interacts with one base molecule. To obtain the content of strong acid sites, the CHA-containing samples dried at 80 °C were further heated in an oven at 250 °C prior to TGA analysis.

RESULTS AND DISCUSSION

Mesostructural Ordering. The XRD patterns of sample MZBN-100 before and after calcination are shown in Figure 1, and the respective basal spacing is given in Table 1. The XRD pattern of as-synthesized MZBN-100 shows a peak at low 2θ value (ca. 1.7°), which we attribute to mesostructural ordering with a basal spacing of 52 Å. In addition, a further weak peak is observed at 2θ = 7°, which is at a position similar to that of the (100) and (101) diffractions of zeolite β. The presence of this second peak suggests either the formation of zeolite β crystallites or the presence of zeolite building units in the as-synthesized MZBN-100 sample. The XRD pattern of calcined MZBN-100 indicates retention of mesostructural ordering (peak at 2θ = 1.8°), with a basal spacing of 49 Å. Calcination therefore induces a slight (ca. 5%) contraction of the as-synthesized sample; such low levels of calcination-induced contraction usually indicate that the as-synthesized silicate framework is at a high level of silica condensation. The XRD pattern of calcined MZBN-100 does not clearly show a peak at 2θ = 7°, which suggests the thermal destruction or diminution of any zeolite β crystallites or zeolite building units. However, given that zeolite β crystallites are known to be stable to calcination,[16] the absence of a clear peak at 2θ = 7° appears to rule out the presence of such crystallites in the MZBN-100 sample.

The XRD patterns indicate that sample MZBN-100 is mesostructured, which is supported by the transmission electron microscopy (TEM) images in Figure 2. The TEM images show relatively well ordered wormhole-type pore channels. The level of pore channel ordering in the TEM images is consistent with the XRD patterns, i.e., the presence of at least one peak.[4,6] Pore channels, of size ca. 30 Å, are observed throughout the particles, and hardly any other phase is observed as might be expected for composite zeolite/mesoporous materials wherein distinct zeolite β crystallites exist.[12,16] The main difference between the present MZBN-100 samples and previous reports that yield zeolite BEA is that we have used a relatively low crystallization temperature (100 °C) and more importantly a higher Si/TEAOH ratio of 2.8. For synthesis gels that yield zeolite BEA phases the Si/TEAOH ratio is usually <2.[13,16] A higher Si/TEAOH ratio is known to delay the growth of zeolite BEA crystallites,[13b] and our results suggest that, under certain conditions, the delay can lead to formation of a mesostructured material via previously suggested mechanisms.[11,12,17] The formation of mesopores in such a scenario is likely to be directed by partially aggregated TEA^+

Table 1. Composition, Textural Properties, and Acidity of Mesoporous Aluminosilicate Materials Prepared from a Zeolite BEA Recipe at a Crystallization Temperature of 100 °C

sample	Si/Al ratio	basal spacing[a] (Å)	surface area ($m^2\ g^{-1}$)	pore volume[b] ($cm^3\ g^{-1}$)	pore size[c] (Å)	acidity[d]
MZBN-100	18.6	49 (52)	527	0.37 (0.06)	25 (35)	0.28 (0.28)
RMZBN-100	13.8		541	0.43 (0.05)	34 (46)	0.47 (0.47)
MZBN-100w3h		94 (100)	667	0.56 (0)	30 (42)	0.22 (0.20)
RMZBN-100w3h			760	0.81 (0)	41 (50)	0.66 (0.65)
MZBN-100w3hd	16.9	83 (88)	649	0.78 (0.04)	52 (62)	0.22 (0.22)
RMZBN-100w3hd	12.7		748	1.08 (0.05)	62 (67)	0.58 (0.53)
MZBN-100w5h	15.9	126	625	0.96 (0.09)	72 (68/87)	0.23 (0.23)
RMZBN-100w5h	12.3		838	1.48 (0.12)	81 (71/88)	0.80 (0.80)

[a] Values in parentheses are the basal spacing of as-synthesized materials. [b] The data in parentheses are micropore volumes. [c] The data in parentheses are pore size maxima obtained using NLDFT analysis. [d] The data in parentheses are strong acidity values after evacuation at 250 °C.

species.[17] Xiao and co-workers have previously observed the formation of mesopores in micro/mesoporous silica generated from $Si/TEA^+/H_2O$ systems that contain partially aggregated TEA^+ species and wherein the concentration of TEA^+ is greater than 6 wt % in water. The nominal concentration of TEA^+ species in our synthesis gel is ca. 14 wt % in water. We therefore propose that TEA^+ species play a role in the initial formation of mesopores in sample MZBN-100.[12c,17] This proposal is consistent with the fact that TEA^+ species are retained in the as-synthesized MZBN-100 mesophase (Figure S1, Supporting Information).[17] The as-synthesized mesophase shows IR peaks at 660−840 cm^{-1} along with peaks at 1635, 1655, 1695, and 1350−1500 cm^{-1} that are attributable to the TEA^+ species.[17]

Figure 1 also shows the low-angle XRD patterns of MZBN-100 derivatives that were washed (i.e., stirred) in boiling water and dried prior to calcination. For materials washed for 3 h (MZBN-100w3h and MZBN-100w3hd), both the as-synthesized and calcined samples exhibit a peak from mesostructural ordering. The basal spacing for as-synthesized samples increases from 52 Å for MZBN-100 to 88 Å for MZBN-100w3hd and to 100 Å for MZBN-100w3h. On calcination, the basal spacing decreases to 83 and 94 Å for MZBN-100w3hd and MZBN-100w3h, respectively, which is a contraction of ca. 6%. The extent of contraction is similar to that of the nonwashed MZBN-100 sample. The amount of water used in the washing step has a slight effect on the extent of the increase in basal spacing, with more water (sample MZBN-100w3h) favoring greater expansion. The as-synthesized sample washed for 5 h (MZBN-100w5h) exhibits an even higher basal spacing of 126 Å. It appears therefore that washing of the as-synthesized mesophase in boiling water causes significant lattice expansion of the MZBN-100 sample. Such expansion of mesoporous silicate mesophases during extended hydrothermal treatment has previously been observed.[18] The expansion/restructuring is caused by thermal effects that act on the relatively flexible as-synthesized aluminosilicate framework under hydrothermal conditions. The observed pore-size expansion involves base-induced intrapore mineralization and transport of aluminosilicate species and redeposition. Dissolution of the aluminosilicate species is made possible by the basic conditions. It is likely that the dissolved aluminosilicate species is transported and redeposited onto areas with a high surface curvature. Similar behavior has been reported for surfactant-templated mesoporous silica.[18c] In such a scenario, the restructuring involves significant dissolution of as-synthesized materials and the subsequent formation, via redeposition, of larger pore materials.

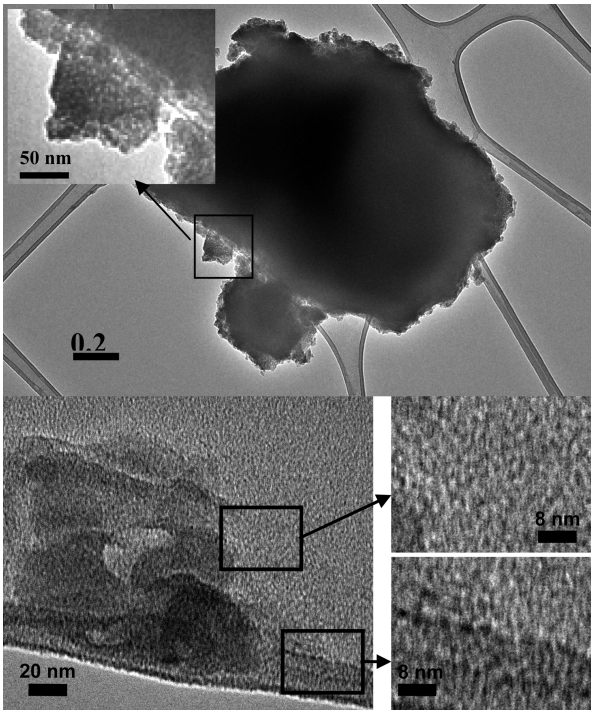

Figure 2. TEM images of calcined MZBN-100.

IR spectra (Figure S1, Supporting Information) show that the lattice expansion which occurs during the washing step is accompanied by removal of some of the TEA^+ species from the as-synthesized mesophase material. IR peaks at 665, 704, 800, 833, and 1403 cm^{-1} arising from the TEA^+ species that are observed for as-synthesized MZBN-100 are not present for the washed samples (Figure S1). Other TEA^+ peaks at 1635, 1655, 1695, and 1350−1500 cm^{-1} also decrease in intensity. The reduction in the TEA content in the washed samples is confirmed by TGA data (Figure S2, Supporting Information). The mass loss associated with decomposition and burnoff of organics (i.e., TEA) between 120 and 350 °C is 38% for as-synthesized MZBN-100, but decreases to ca. 17% and 15% for samples washed for 3 h (MZBN-100w3h and MZBN-100w3hd) and 5 h (MZBN-100w5h), respectively. Furthermore, we also observed that the amount of water in as-synthesized MZBN-100 (according to TGA mass loss up to 100 °C as shown in Figure S2) was 1.2 wt % compared to ca. 6.5 wt % for the washed larger

dx.doi.org/10.1021/cm200706n |Chem. Mater. 2011, 23, 2491–2498

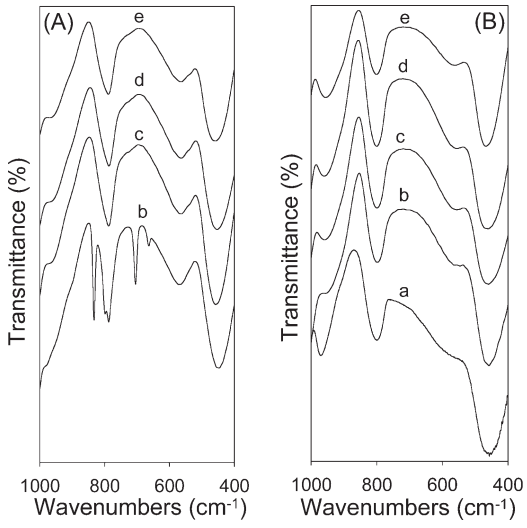

Figure 3. Infrared spectra of (A) as-synthesized and (B) calcined aluminosilicate materials prepared from a zeolite BEA recipe: (b) MZBN-100, (c) MZBN-100w3h, (d) MZBN-100w3hd, (e) MZBN-100w5h, and for comparison (a) calcined Al-MCM-41.

pore samples. This implies that the additional space created during pore size expansion is occupied by water. Indeed, the amount of occluded water as a proportion of the surfactant-free aluminosilicate framework (residual mass at 800 °C) increases from 2.2 wt % for MZBN-100 to ca. 9.0 wt % for the washed larger pore samples.

Framework Ordering. To further probe the nature of the framework in the MZBN-100 sample and the washed derivatives, we performed IR spectroscopy analysis on the as-synthesized and calcined samples. IR analysis is a good probe for the presence of zeolite-like building units in mesoporous materials.[19,20] Figure 3A shows IR spectra of as-synthesized MZBN-100 and the washed derivatives. All the samples exhibit a well-developed IR band at ca. 580 cm^{-1}, indicative of six- or five-membered ring subunits of T−O−T (T = Si or Al) similar to subunits found in zeolites.[19] The IR peak observed for the MZBN-100 samples is similar to that previously reported for mesoporous materials that possess zeolite building units.[19,20] The zeolite building units do not appear to be adversely affected by washing prior to calcination. Furthermore, as shown in Figure 3B, the peak at ca. 580 cm^{-1} is still observed for calcined samples although with reduced intensity. The peak at 580 cm^{-1} is not observed in the IR spectra of a conventional calcined Al-MCM-41 sample (Figure 3B). The spectra in Figure 3 clearly show a distinction between the MZBN-*X* samples and conventional mesoporous materials (e.g., Al-MCM-41) that do not possess zeolite building units.

To assess the extent of silicate condensation in the as-synthesized samples, we performed Si MAS NMR. The ^{29}MAS NMR spectra, shown in Figure 4, exhibit three resonances at −90 ppm (Q^2), −100 ppm (Q^3), and −109 ppm (Q^4). The resonances are assigned to silicon in the $Si(OSi)_2(OH)_2$ (Q^2), $Si(OSi)_3OH$ (Q^3), or $Si(OSi)_4$ (Q^4) environment. We note that there may also be Si in $Si(OSi)_2(OAl)(OH)$ (−90 ppm) and $Si(OSi)_3(OAl)$ (−100 ppm) environments. Overall, the intensity of the resonances indicates that most of the Si is in Q^3 and Q^4 sites, with a greater proportion in the Q^3 sites. The $Q^4/(Q^3 + Q^2)$ ratio was used to estimate the extent of silicate condensation, with a higher ratio indicating a more condensed framework. The

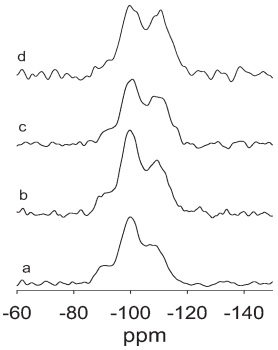

Figure 4. ^{29}Si MAS NMR spectra of as-synthesized aluminosilicate materials prepared from a zeolite BEA recipe: (a) MZBN-100, (b) MZBN-100w3hd, (c) MZBN-100w3h, (d) MZBN-100w5h.

$Q^4/(Q^3 + Q^2)$ ratios are 0.48 (MZBN-100), 0.70 (MZBN-100w3hd), 0.79 (MZBN-100w3h), and 0.92 for MZBN-100w5h. The trend in the ratio indicates that further silicate condensation occurred during the washing step and that the longer the washing duration, the greater the extent of condensation. The changes in extent of silicate condensation are consistent with the lattice expansion (Figure 1) and removal of TEA^+ species (Figure S1, Supporting Information), which occurs during washing in boiling water. These changes involve expansion of the forming aluminosilicate framework, whereby dissolved Si and Al species enable further growth and condensation.

Al Content and Acidity. The Al content of the samples is given as the Si/Al ratio in Table 1. Sample MZBN-100 has a Si/Al ratio of 18.6, which is lower than the synthesis gel ratio of 25. This indicates that Al was preferentially incorporated into the aluminosilicate material, which is a common phenomenon for direct (i.e., sol−gel) synthesized mesoporous and microporous (zeolite) aluminosilicates.[13,21] In all cases, washing of as-synthesized sample MZBN-100 resulted in an increase in the Al content (i.e., the Si/Al ratio decreased from 18.6 to between 15.9 and 16.9). As noted above, washing in boiling water caused expansion of the aluminosilicate framework via dissolution and redeposition of silicate and aluminate species. This reconstruction appears to cause the loss of some Si and/or the preferential redeposition of Al. The ^{27}Al MAS NMR spectra of the samples, before and after calcination, are shown in Figure 5. The spectrum of as-synthesized MZBN-100 exhibits only one sharp resonance at ca. 53 ppm, which arises from tetrahedrally coordinated Al in the aluminosilicate framework. This indicates that all Al in the as-synthesized MZBN-100 sample existed within the framework and that there was no extraframework (octahedrally coordinated) Al. The spectrum of calcined MZBN-100 also exhibits one resonance at 53 ppm, which indicates that calcination did not cause any dealumination. Sample MZBN-100 was therefore stable to calcination similarly to zeolites and unlike conventional mesoporous aluminosilicates.[3−6,21] Washing of as-synthesized MZBN-100 caused the formation of extraframework Al as indicted by the peak at ca. 10 ppm for samples MZBN-100w3hd, MZBN-100w3h, and MZBN-100w5h. Most of the extraframework Al in the washed as-synthesized samples is however reinserted into the framework during calcination.

The overall picture that emerges from the ^{27}Al MASNMR spectra is that the Al in calcined samples is predominantly within framework positions. Such framework Al is expected to generate acid sites as shown by the acidity data in Table 1. The samples have

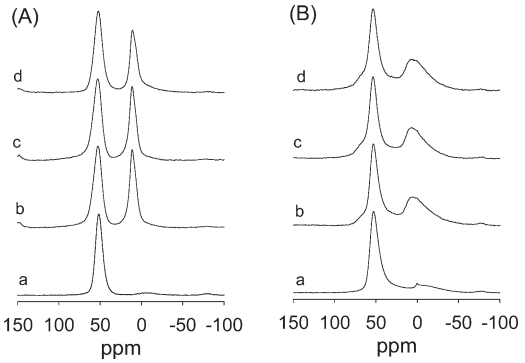

Figure 5. ^{27}Al MAS NMR spectra of (A) as-synthesized and (B) calcined mesoporous aluminosilicate materials prepared from a zeolite BEA recipe: (a) MZBN-100, (b) MZBN-100w3hd, (c) MZBN-100w3h, (d) MZBN-100w5h.

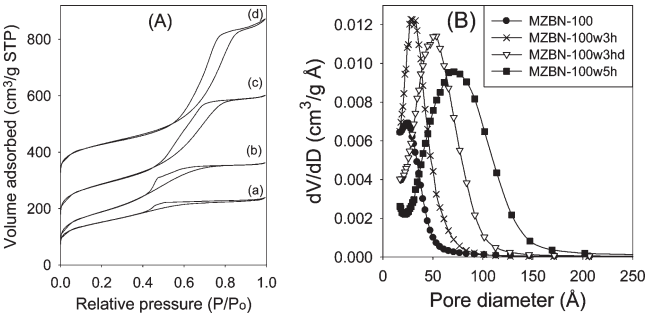

Figure 6. Nitrogen sorption isotherms (A) and corresponding pore size distribution curves (B) of mesoporous aluminosilicate materials prepared from a zeolite BEA recipe: (a) MZBN-100, (b) MZBN-100w3h, (c) MZBN-100w3hd, (d) MZBN-100w5h. For clarity isotherms c and d are offset (y-axis) by 100 and 250 cm^3/g, respectively.

comparable acidity, with slightly higher acid content for the nonwashed MZBN-100 sample. This is consistent with the NMR spectra in Figure 5, i.e., that sample MZBN-100 has the highest content of framework Al. Although the washed samples have a higher overall Al content (i.e., lower Si/Al ratio), some of the Al is in extraframework sites that do not generate acid sites. What is however unexpected is that in all cases the total acidity and strong acidity values are similar, i.e., that the samples mainly possess strong acid sites. This is different from conventional mesoporous aluminosilicates, which usually possess a much lower proportion of strong acid sites.[21b,22] We attribute the strong acidity to the presence of zeolite building units in the MZBN-100 samples in a manner similar to that observed for composite micro/mesoporous materials.[12d]

Porosity. The nitrogen sorption isotherms of calcined MZBN-100 samples are shown in Figure 6A, and the textural properties are summarized in Table 1. Sample MZBN-100 shows a type IV isotherm with a mesopore filling step in the relative pressure (P/P_o) range of 0.4−0.6, thus confirming the presence of mesoporosity. The pore size distribution curves (obtained via BJH analysis of adsorption isotherm data) in Figure 6B show relatively uniform pores of size ca. 25 Å for sample MZBN-100. Analysis of the pore size distribution using an NLDFT method (Figure S3, Supporting Information) indicated a pore size of ca. 35 Å (Table 1) for sample MZBN-100. The disparity between the two methods is not unexpected since the BJH model is known to underestimate the pore size of mesoporous materials.[23] Nevertheless, the pore size (25−35 Å) calculated from the nitrogen sorption data is similar to that (ca. 30 Å) obtained from the TEM images (Figure 2). The surface area (527 m^2/g) and pore volume (0.37 cm^3/g) of sample MZBN-100 are within the lower range expected for mesoporous materials.[4,6] The relatively low textural properties of sample MZBN-100 may be attributed to the presence of zeolite units within the aluminosilicate framework, which increases the framework density as previously reported.[10,20b,24] The extent of microporosity in sample MZBN-100 is important given that it was prepared from a zeolite recipe. The micropore volume (0.06 cm^3/g) contributes 16% of the total pore volume (Table 1), which suggests that sample MZBN-100 is predominantly mesoporous. The low level of microporosity is confirmed by the NLDFT pore size distribution (Figure S3), which shows very few pores with a diameter smaller than 20 Å. These observations are at variance with what might be expected for a composite micro/mesomaterial with a separate zeolite component.[16,25]

The nitrogen sorption isotherms of samples washed prior to calcination exhibit well-developed mesoporosity with a mesopore filling step in the relative pressure (P/P_o) range of 0.4−0.8. The mesopore filling step is shifted to higher partial pressure depending on the washing duration. Furthermore, the height of the mesopore filling step increases for longer washing duration, which is an indication of greater mesoporosity. The changes in porosity caused by washing are two-fold: (i) increase in pore size as shown in Figure 6B (and Figure S3, Supporting Information) and (ii) greater mesoporosity along with associated increases in surface area and pore volume. The pore size increases from ca. 30 Å for sample MZBN-100 to ca. 40 and 55 Å for MZBN-100w3h and MZBN-100w3hd, respectively, and 72 Å for MZBN-100w5h. It is interesting that sample MZBN-100w3h has a smaller pore size (compared to MZBN-100w3hd) despite a larger basal spacing. This may suggest that sample MZBN-100w3h has thicker pore walls and that low amounts of water during the washing step (sample MZBN-100w3hd) favor expansion of the pore size over formation of thicker walls as the aluminosilicate framework is restructured. The increase in pore size is accompanied by a small rise in surface area (from 527 m^2/g for MZBN-100 to between 625 and 667 m^2/g for the washed samples) and much larger increases in pore volume from 0.37 to between 0.56 and 0.96 cm^3/g. It is also noteworthy that after washing the proportion of microporosity generally decreases, and in some cases (e.g., sample MZBN-100w3h) decreases to nil. The washing step therefore provides a route to modifying the textural properties of the present aluminosilicate samples.

Effect of the Crystallization Temperature. To clarify the effect of the Si/TEAOH ratio and crystallization temperature, and to gain further information on the mechanism of formation of MZBN materials, we performed synthesis at temperatures higher than 100 °C (i.e., 135 and 150 °C) and lower than 100 °C (i.e., 25, 50, and 80 °C). Synthesis at 135 °C (sample MZBN-135) generated a large-pore mesoporous material (Figure 7). Sample MZBN-135 has a surface area of 468 m^2/g (Table S1, Supporting Information), which is comparable to that of sample MZBN-100, but double the pore volume (0.70 cm^3/g compared to 0.37 cm^3/g). This is due to the fact that the pore size of MZBN-135 (118 Å) is, as shown in Figure 7 (and Figure S4, Supporting Information), at least 3 times as large as that of MZBN-100 (Tables 1 and S1). Washing of sample MZBN-135 prior to calcination only slightly increases the pore size to ca. 140 Å (Figure 7, Table S1, Figure S4). The proportion of micropore

dx.doi.org/10.1021/cm200706n |Chem. Mater. 2011, 23, 2491–2498

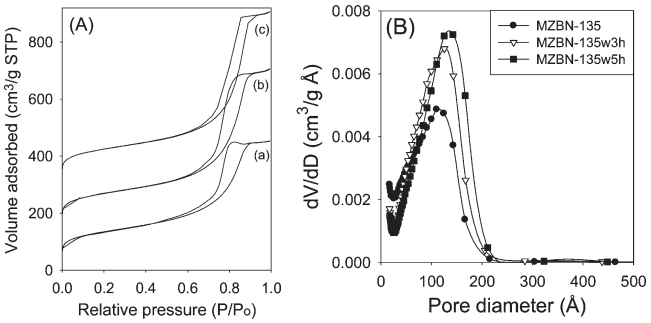

Figure 7. Nitrogen sorption isotherms (A) and corresponding pore size distribution curves (B) for mesoporous aluminosilicate materials prepared from a zeolite BEA recipe at 135 °C: (a) MZBN-135, (b) MZBN-135w3h, (c) MZBN-135w5h. For clarity in (A) isotherms b and c are offset (*y*-axis) by 100 and 250 cm^3/g, respectively.

volume (ca. 0.1 cm^3/g) for MZBN-135 samples is ca. 12% of the total pore volume, which is comparable to that of MZBN-100. Crystallization at 135 °C therefore directly generates large-pore mesoporous materials even without the washing step. It is however noteworthy that, despite the higher temperature, the final phase is still a mesoporous rather than zeolitic microporous phase. We propose that the higher crystallization temperature increases the rate of formation of zeolite building units and speeds up their incorporation into a growing mesostructured aluminosilicate network "templated" by TEA species via a scaffolding mechanism.[11] Once formed, the growing aluminosilicate framework undergoes expansion (in a manner similar to that proposed above for the MZBN-100 sample) during the extended crystallization at 135 °C to generate a stable mesoporous framework with larger pores. IR spectra (Figure S5, Supporting Information) indicated that the extent to which zeolite units are present in sample MZBN-135 (IR peak at ca. 580 cm^{-1}) is similar to that of sample MZBN-100 (Figure 3).

On the other hand, synthesis at 150 °C (sample MZBN-150) generated a rather poorly ordered material with a wide pore size distribution (Figure S6, Supporting Information). The MZBN-150 sample has a surface area of 592 m^2/g (Table S1) and a pore volume of 0.64 cm^3/g. Washing of sample MZBN-150 prior to calcination slightly reduces the surface area, pore volume, and mesoporosity (Table S1). It is noteworthy that the micropore volume (ca. 0.2 cm^3/g) for MZBN-150 samples is 30−40% of the total pore volume, which is a much higher proportion than that of samples prepared at 100 and 135 °C. The significant proportion of microporosity in MZBN-150 samples was confirmed by the NLDFT pore size distribution (Figure S6C). It appears therefore that crystallization at a much high temperature (i.e., 150 °C) shifts the final material toward being microporous rather than mesoporous. Indeed the porosity of the MZBN-150 samples is similar to that of aggregated zeolite β nanocrystals.[14] It is therefore likely that crystallization at 150 °C speeds up the rate of formation of zeolite β nanocrystals. We propose that crystallization at 150 °C speeds up the rate of formation of zeolite β nanocrystals, whereby the higher temperature balances out the inhibiting effect of the high Si/TEAOH ratio.[13b] Faster growth of zeolite β nanocrystals inhibits formation of a mesostructured material, thus shifting the final material toward a microporous zeolite phase as observed from the porosity data (Figure S6 and Table S1). Indeed the XRD patterns of sample MZBN-150 (Figure S7, Supporting Information) indicate the formation of a zeolite β material. Futhermore, the IR

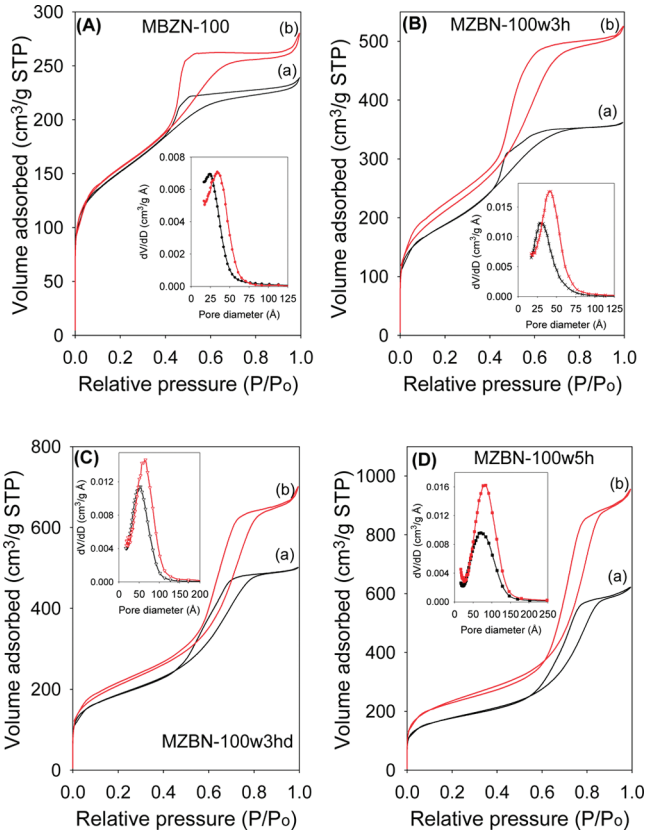

Figure 8. Nitrogen sorption isotherms and corresponding pore size distribution curves (inset) of calcined MZBN-100 samples before (a) and after (b) refluxing in water: (A) MZBN-100, (B) MZBN-1003wh, (C) MZBN-100w3hd, (D) MZBN-100w5h.

spectrum of sample MZBN-150 (Figure S8, Supporting Information) is fully consistent with the formation of a zeolitic material, with several IR peaks between 400 and 600 cm^{-1} arising from well-formed zeolite β crystallites.[13,19] The data from the 135 and 150 °C samples, when compared to sample MZBN-100, mean that there needs to be a balance between the Si/TEAOH ratio and crystallization temperature to obtain mesoporous materials. This assertion is supported by the fact that MZBN-*X* materials prepared at 80 °C (Figure S9, Supporting Information) and 50 °C (Figure S10, Supporting Information) are both mesoporous and their textural properties are similar to those of sample MZBN-100 (Table S2, Supporting Information). IR spectra (Figure S11, Supporting Information) indicated that the extent to which zeolite units are present in sample MZBN-50 (IR peak at ca. 580 cm^{-1}) is rather lower than that of sample MZBN-100 (Figure 3) and MZBN-135 (Figure S5). Crystallization at a lower temperature of 25 °C (Figure S12, Supporting Information) generated MZBN-25 porous materials with a wide pore size distribution. Washing of sample MZBN-25 prior to calcination broadened the pore size distribution even further. However, MZBN-25 samples had a surface area and pore volume comparable to those of samples prepared at higher temperature (Tables 1, S1, and S2). Our data therefore suggest that mesostructured aluminosilicate materials may be obtained from the zeolite BEA recipe for synthesis temperatures between 50 and 135 °C. The pore size generally increases with synthesis temperature, although it can also be modified by washing prior to calcination. A higher crystallization

dx.doi.org/10.1021/cm200706n |*Chem. Mater.* 2011, 23, 2491–2498

temperature of 150 °C generates a predominantly microporous zeolite β material. The crystallization temperature does not, however, have any significant affect on the Si/Al ratio (Tables 1, S1, and S2).

Hydrothermal Stability. One of the advantages of zeolites over mesoporous silicates is their higher hydrothermal stability. Hydrothermal stability is an important property for porous aluminosilicates since many of their applications may require use in hot aqueous media.[1,2,5] We assessed the hydrothermal stability of MZBN-100 samples by refluxing in water for 6 or 120 h. Figure 8 shows the nitrogen sorption isotherms of the samples before and after 6 h of refluxing in water. It is clear that all the samples exhibit high hydrothermal stability; the isotherms of the refluxed samples exhibit a well-developed mesopore filling step characteristic of well-ordered mesoporous materials. Furthermore, in all cases the height of the mesopore filling step increases after refluxing. The hydrothermal treatment therefore enhances the mesoporosity, which is a rather unusual observation since most mesostructured aluminosilicates undergo some diminution of mesoporosity when refluxed in water.[5,19,26]

The textural parameters of the samples after hydrothermal treatment are given in Table 1. In all cases, the hydrothermal treatment results in an increase in pore size while still retaining a narrow pore size distribution as shown in Figure 8. (We note that the sum effect of washing the as-synthesized material, in combination with refluxing after calcination, is that the pore size of sample MZBN-100 can be tailored between 25 and 88 Å.) The surface area increases after refluxing, with sample MZBN-100w5h exhibiting the greatest increase (35%) from 625 to 838 m^2/g. The pore volume also shows increases of 16% for MZBN-100, ca. 40% for MZBN-100w3h and MZBN-100w3hd, and 54% for MZBN-100w5h. The proportion of microporosity is not affected by refluxing. Extending the hydrothermal testing (refluxing) time to 120 h had no effect on the mesoporosity of the materials (Figure S13, Supporting Information). Sample MZBN-100 refluxed for 120 h had a surface area of 506 m^2/g and a pore volume of 0.4 cm^3/g, with a micropore volume of 0.03 cm^3/g. These values are similar to those of the parent MZBN-100, which attests to the high hydrothermal stability of the MZBN-*X* aluminosilicate materials.

The Si/Al ratio of the samples decreases after refluxing as shown in Table 1. The Al content per gram of material increases for the refluxed samples by ca. 30% due to removal of amorphous silica during refluxing. Removal of amorphous silica (which is not part of the mesoporous aluminosilicate structure) would explain both the increase in Al content and the textural changes. If such silica is within the pores, removal would lead to an apparent increase in pore size and pore volume as observed. The ^{27}Al MAS NMR spectra of the MZBN-100 samples do not change after refluxing (Figure 9), exhibiting a sharp resonance at ca. 53 ppm from tetrahedrally coordinated Al in the aluminosilicate framework and a low-intensity resonance at ca. 5 ppm from octahedrally coordinated nonframework Al. The ratio of tetrahedral to octahedral Al is unaffected by the refluxing (compare Figures 5 and 9). This indicates that refluxing does not cause any dealumination, meaning that MZBN-type materials are stable to hydrothermal treatment (refluxing), which is unlike conventional mesoporous aluminosilicates.[3−6,21] The acidity of the refluxed samples increases significantly and in most cases more than doubles as shown in Table 1. The increase in acidity per weight of sample is not unexpected given that the Al content increases and the fact that the refluxing causes no dealumination.

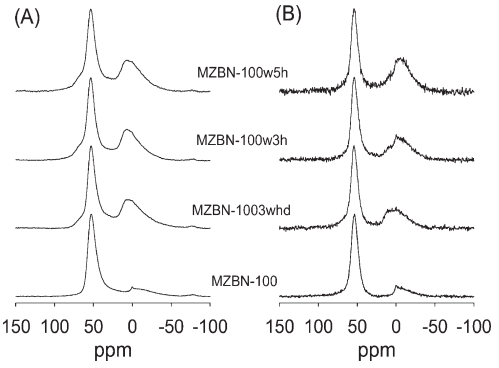

Figure 9. ^{27}Al MAS NMR spectra of calcined mesoporous aluminosilicate materials prepared from a zeolite BEA recipe before (A) and after (B) refluxing in water for 6 h: (a) MZBN-100, (b) MZBN-100w3hd, (c) MZBN-100w3h, (d) MZBN-100w5h.

However, the increase in acidity is much higher than the rise in Al content, which indicates that some of the acid sites may have been blocked by silica before refluxing. Removal of the silica not only increases the acid content per given weight of sample but also unblocks some acid sites. Overall, the data of the refluxed samples show that the MZBN-type materials are very stable to hydrothermal treatment.

CONCLUSIONS

In summary, we have shown that a zeolite recipe may be used to prepare strongly acidic and hydrothermally stable mesoporous aluminosilicates that have potential for use as solid acid catalysts or catalyst supports. The mesoporous aluminosilicates are obtained from a recipe typically used for the synthesis of zeolite BEA but at relatively low crystallization temperature and a high Si/TEAOH ratio. The porosity of the aluminosilicates is readily modified by washing the as-synthesized mesophase in boiling water prior to calcination. This allows preparation of mesoporous aluminosilicates with surface areas of 500−850 m^2/g, pore volumes in the range of 0.35−1.5 cm^3/g, and pore sizes between 25 and 140 Å. The synthesis route reported here avoids the use of surfactant templates and directly generates acid sites on calcination.

ASSOCIATED CONTENT

Supporting Information. Two tables with textural and elemental composition data for samples prepared at 150, 135, 80, 50, and 25 °C and twelve additional figures showing infrared spectra of as-synthesized mesophases and calcined materials, thermogravimetric analysis curves of as-synthesized mesophases, NLDFT pore size distribution curves of samples prepared at 100 and 135 °C, nitrogen sorption and pore size distribution curves of samples prepared at 150, 80, 50, and 25 °C, powder XRD pattern of a sample prepared at 150 °C, and nitrogen sorption isotherms and pore size distribution curves of sample MZBN-100 after being refluxed for 120 h (PDF). This material is available free of charge via the Internet at http://pubs.acs.org.

AUTHOR INFORMATION

Corresponding Author

*E-mail: r.mokaya@nottingham.ac.uk.

■ ACKNOWLEDGMENT

We thank Dr. David Apperley at the Engineering and Physical Sciences Research Council Solid State NMR Service (Durham, U.K.) for the NMR spectra and are grateful to Dr. Andrei Khlobystov for assistance with the TEM images.

■ REFERENCES

(1) Corma, A. *Chem. Rev.* **1997**, *97*, 2373.
(2) Davis, M. E. *Nature* **2002**, *417*, 813.
(3) Kresge, C. T.; Leonowicz, M. E.; Roth, W. J.; Vartuli, J. C.; Beck, J. S. *Nature* **1992**, *359*, 710. (b) Beck, J. S.; Vartuli, J. C.; Roth, W. J.; Leonowicz, M. E.; Kresge, C. T.; Schmitt, K. D.; Chu, C. T.-W.; Olson, D. H.; Sheppard, E. W.; McCullen, S. B.; Higgins, J. B.; Schlenker, J. L. *J. Am. Chem. Soc.* **1992**, *114*, 10834.
(4) Ying, J. Y.; Mehnert, C. P.; Wong, M. S. *Angew. Chem., Int. Ed.* **1999**, *38*, 56. (b) Øye, G.; Sjöblom, J.; Stöcker, M. *Adv. Colloid Interface Sci.* **2001**, *89*, 439. (c) On, D. T.; Desplantier-Giscard, D.; Danumah, C.; Kaliaguine, S. *Appl. Catal., A* **2002**, *222*, 299.
(5) Liu, Y.; Pinnavaia, T. J. *J. Mater. Chem.* **2002**, *12*, 3179.
(6) (a) Taguchi, A.; Schuth, F. *Microporous Mesoporous Mater.* **2005**, *77*, 1. (b) Pega, S.; Boissiere, C.; Grosso, D.; Azais, T.; Chaumonnot, A.; Sanchez, C. *Angew. Chem., Int. Ed.* **2009**, *48*, 2784.
(7) Christiansen, S. C.; Zhao, D. Y.; Janicke, M. T.; Landry, C. C.; Stucky, G. D.; Chmelka, B. F. *J. Am. Chem. Soc.* **2001**, *123*, 4519.
(8) Wang, L. Q.; Exarhos, G. J. *J. Phys. Chem. B* **2003**, *107*, 443.
(9) (a) Mokaya, R. *Chem. Commun.* **2001**, 1092. (b) Xia, Y.; Titman, J. J.; Mokaya, R. *J. Phys. Chem. B* **2004**, *108*, 11361. (c) Xia, Y.; Mokaya, R. *Microporous Mesoporous Mater.* **2006**, *94*, 295. (d) Xia, Y.; Mokaya, R. *J. Phys. Chem. B* **2006**, *110*, 9122.
(10) (a) Choi, M.; Cho, H. E.; Srivastava, R.; Venkatesan, C.; Choi, D. H.; Ryoo, R. *Nat. Mater.* **2006**, *5*, 718. (b) Srivastava, R.; Choi, M.; Ryoo, R. *Chem. Commun.* **2006**, 4489. (c) Shetti, V. N.; Kim, J.; Srivastava, R.; Choi, M.; Ryoo, R. *J. Catal.* **2008**, *254*, 296.
(11) Jansen, J. C.; Shan, Z.; Marchese, L.; Zhou, W.; Puil, N. V. D.; Maschmeyer, T. *Chem. Commun.* **2001**, 713.
(12) (a) Wang, J.; Groen, J. C.; Yue, W.; Zhou, W.; Coppens, M. O. *Chem. Commun.* **2007**, 4653. (b) Wang, J.; Groen, J. C.; Yue, W.; Zhou, W.; Coppens, M. O. *J. Mater. Chem.* **2008**, *18*, 468. (c) Wang, J.; Groen, J. C.; Coppens, M. O. *J. Phys. Chem. C* **2008**, *112*, 19336. (d) Wang, J.; Yue, W.; Zhou, W.; Coppens, M. O. *Microporous Mesoporous Mater.* **2009**, *120*, 19.
(13) (a) Gautier, B.; Smaihi, M. *New J. Chem.* **2004**, *28*, 457. (b) Camblor, M. A.; Mifsud, A.; Perez-Pariente, J. *Zeolites* **1991**, *11*, 792. (c) Camblor, M. A.; Perez-Pariente, J. *Zeolites* **1991**, *11*, 202.
(14) Mokaya, R.; Jones, W.; Moreno, S.; Poncelet, G. *Catal. Lett.* **1997**, *49*, 87.
(15) Breen, C. *Clay Minerals* **1991**, *26*, 487.
(16) (a) Xiao, F. S.; Wang, L.; Yin, C.; Lin, K.; Di, Y.; Li, J.; Xu, R.; Su, D. S.; Schlogl, R.; Yokoi, T.; Tatsumi, T. *Angew. Chem., Int. Ed.* **2006**, *45*, 3090. (b) Wang, H.; Pinnavaia, T. J. *Angew. Chem., Int. Ed.* **2006**, *45*, 7603. (c) Song, J.; Ren, L.; Yin, C.; Ji, Y.; Wu, Z.; Li, J.; Xiao, F. S. *J. Phys. Chem. C* **2008**, *112*, 8609. (d) Wang, L.; Zhang, Z.; Yin, C. Y.; Shan, Z.; Xiao, F. S. *Microporous Mesoporous Mater.* **2010**, *131*, 58. (e) Gu, F. N.; Wei, F.; Yang, J. Y.; Lin, N.; Lin, W. G.; Wang, Y.; Zhu, J. H. *Chem. Mater.* **2010**, *22*, 2442.
(17) Ji, Y.; Wang, C.; Zou, Y.; Song, J.; Wang, J.; Li, F.; Xiao, F. S. *J. Phys. Chem. C* **2008**, *112*, 19367.
(18) (a) Sayari, A.; Liu, P.; Kruk, M.; Jaroniec, M. *Chem. Mater.* **1997**, *9*, 2499. (b) Chen, L. Y.; Horiuch, T.; Mori, T.; Maeda, K. *J. Phys. Chem. B* **1999**, *103*, 1226. (c) Cheng, C. F.; Zhou, W. Z.; Klinowski, J. *Chem. Phy. Lett.* **1996**, *263*, 247. (d) Mokaya, R. *J. Phys. Chem. B* **1999**, *103*, 10204. (e) Khushalani, D.; Kuperman, A.; Ozin, G. A.; Tanaka, K.; Garces, J.; Olken, M. A.; Coombs, N. *Adv. Mater.* **1995**, *7*, 845.
(19) (a) Liu, Y.; Zhang, W.; Pinnavaia, T. J. *J. Am. Chem. Soc.* **2000**, *122*, 8791. (b) Liu, Y.; Zhang, W.; Pinnavaia, T. J. *Angew. Chem., Int. Ed.* **2001**, *40*, 1255. (c) Zhang, Z.; Han, Y.; Zhu, L.; Wang, R.; Yu, Y.; Qiu, S.; Zhao, D.; Xiao, F.-S. *Angew. Chem., Int. Ed.* **2001**, *40*, 1258. (d) Zhang, Z.; Han, Y.; Xiao, F-S; Qiu, S.; Zhu, L.; Wang, R.; Yu, Y.; Zou, B.; Wang, Y.; Sun, H.; Zhao, D.; Wei, Y. *J. Am. Chem. Soc.* **2001**, *123*, 5014. (e) Liu, J.; Zhang, X.; Han, Y.; Xiao, F. S. *Chem. Mater.* **2002**, *14*, 2536.
(20) (a) Xia, Y.; Mokaya, R. *J. Mater. Chem.* **2004**, *14*, 3427. (b) Alam, N.; Mokaya, R. *J. Mater. Chem.* **2008**, *18*, 1383.
(21) (a) Biz, S.; White, M. G. *J. Phys. Chem. B* **1999**, *103*, 8432. (b) Mokaya, R.; Jones, W. *J. Mater. Chem.* **1998**, *8*, 2819. (c) Mokaya, R. *J. Phys. Chem. B* **2000**, *104*, 8279. (d) Xia, Y.; Mokaya, R. *J. Phys. Chem. B* **2003**, *107*, 6954.
(22) Mokaya, R.; Jones, W. *Phys. Chem. Chem. Phys.* **1999**, *1*, 207.
(23) (a) Ravikovitch, P. I.; Domhnaill, S. C. O.; Neimark, A. V.; Schuth, F.; Unger, K. K. *Langmuir* **1995**, *11*, 4765. (b) Lastoskie, C.; Gubbins, K. E.; Quirke, N. *J. Phys. Chem.* **1993**, *97*, 4786. (c) Kruk, M.; Jaroniec, M.; Sayari, A. *J. Phys. Chem. B* **1997**, *101*, 583.
(24) Fang, Y.; Hu, H. *J. Am. Chem. Soc.* **2006**, *128*, 10636.
(25) Xia, Y.; Mokaya, R. *J. Mater. Chem.* **2004**, *14*, 863.
(26) (a) Stein, A. *Adv. Mater.* **2003**, *15*, 763. (b) Pan, D.; Yuan, P.; Zhao, L.; Liu, N.; Zhou, L.; Wei, G.; Zhang, J.; Ling, Y.; Fan, Y.; Wei, B.; Liu, H.; Yu, C.; Bao, X. *Chem. Mater.* **2009**, *22*, 5413. (c) Mokaya, R. *Angew. Chem., Int. Ed.* **1999**, *38*, 2930. (d) Mokaya, R. *Adv. Mater.* **2000**, *12*, 1681. (e) Mokaya, R. *Chem. Commun.* **2001**, 633.